CHAPTER V

NON-ISOTHERMAL COLD-CRYSTALLIZATION KINETICS OF POLY(TRIMETHYLENE TEREPHTHALATE)

ABSTRACT

Non-isothermal cold-crystallization kinetics and subsequent melting behavior of poly(trimethylene terephthalate) (PTT) have been investigated by differential scanning calorimetry (DSC) technique. The Avrami, Tobin and Ozawa equations were applied to describe the kinetics of the crystallization process. Both of the Avrami and Tobin crystallization rate parameters (i.e. K_A and K_T, respectively) were found to increase with increasing heating rate. The Ozawa crystallization rate K_O was found to increase with increasing temperature. The ability of PTT to crystallize from the glassy state under a unit cooling rate was determined by the Ziabicki's kinetic crystallizability index, which was found to be ca. 0.89. The effective energy barrier describing the non-isothermal cold-crystallization process of PTT was estimated by the differential iso-conversional method of Friedman and was found to range between ca. 114.5 and 158.8 $kJ \cdot mol^{-1}$. In its subsequent melting, PTT exhibited double melting behavior for heating rates lower than or equal to $10°C \cdot min^{-1}$ and single melting behavior for heating rates greater than or equal to $12.5°C \cdot min^{-1}$.

(**Key-words:** poly(trimethylene terephthalate); non-isothermal cold-crystallization behavior; subsequent melting behavior)

1. INTRODUCTION

Poly(trimethylene terephthalate) (PTT) is a linear aromatic polyester which was first synthesized by Whinfield and Dickson in 1941 [1]. At that time, it was not available commercially because of the high production cost of one of the main reactants, 1,3-propanediol (PDO). With recent breakthroughs in PDO synthesis via hydroformylation of ethylene oxide, process improvements in traditional synthetic route through acrolein, and promising bioengineering route that helped reduce its production cost [2], commercial production of PTT could then be realized. Prospective uses for PTT are in areas such as fibers, films, and engineering thermoplastics. Mechanical properties of PTT lie roughly between those of poly(ethylene terephthalate) (PET) and poly(buthylene terephthalate) (PBT). Of interest is that PTT showed a better tensile elastic recovery and a lower modulus than PET and PBT [3]. These two properties are very desirable for making soft, stretchable fabrics with good toughability [4].

Semi-crystalline polymers can crystallize between their glass transition temperature T_g and their apparent melting temperature T_m. The bulk crystallization process can be classified into two categories, depending on the initial state from which the polymers are brought to crystallize. If the polymers are brought to crystallize from the molten state (i.e. from a temperature higher than T_m), it is called melt-crystallization. On the contrary, if the polymers are brought to crystallize from the glassy state (i.e. from a temperature lower than T_g), it is called cold-crystallization. Studies related to melt-crystallization of polymers are abundant in the literature, while studies related to cold-crystallization are much less frequent [5,6].

It is known that both physical and mechanical properties of semi-crystalline polymers are strongly depended on the extent of crystallization and the morphology developed during processing, studies related to crystallization kinetics are key information to gain an understanding on the relationship among the processing conditions, the structure developed, and the properties obtained in the final products. Investigations related to chain conformation, crystal structure, and morphology of PTT have been carried out and reported in recent years [7-9]. A few studies related to the subject of isothermal melt-crystallization kinetics of PTT include Avrami

crystallization kinetics [10-14] and the kinetics of the linear spherulitic growth rates [11,12,15]. We have earlier reported some information about non-isothermal melt-crystallization kinetics of PTT in comparison with PET and PBT [16] and non-isothermal melt-crystallization kinetics of PTT and its blends with PBT [17].

Very recently, we have reported a thorough study on non-isothermal melt-crystallization kinetics of PTT [18]. The Avrami, Tobin and Ozawa equations were applied to describe the kinetics of the crystallization process. Both of the Avrami and Tobin crystallization rate parameters were found to increase with increasing cooling rate. The Ozawa crystallization rate was found to decrease with increasing temperature. The ability of PTT to crystallize from the melt under a unit cooling rate was determined by the Ziabicki's kinetic crystallizability index, which was found to be ca. 0.98. The effective energy barrier describing the non-isothermal melt-crystallization process of PTT was estimated by the differential iso-conversional method of Friedman and was found to increase with an increase in the relative crystallinity.

In the present contribution, the overall kinetics of non-isothermal cold-crystallization of PTT was thoroughly investigated, for the first time, using differential scanning calorimetry (DSC) technique. The experimental data were analyzed based on the Avrami, Tobin, Ozawa, and Ziabicki macrokinetic models. The activation energy describing the non-isothermal cold-crystallization process of PTT was evaluated based on the differential iso-conversional method of Friedman.

2. THEORITICAL BACKGROUND

In DSC, the energy released during non-isothermal crystallization process appears to be a function of temperature rather than time as in the case of isothermal crystallization process. As a result, the relative crystallinity as a function of temperature $\theta(T)$ can be formulated as

$$\theta(T) = \frac{\int_{T_0}^{T} \left(\frac{dH_c}{dT} \right) dT}{\Delta H_c}, \tag{1}$$

where T_0 and T represent the onset and an arbitrary temperature, respectively, dH_c is the enthalpy of crystallization released during an infinitesimal temperature range dT,

and ΔH_c is the total enthalpy of crystallization for a specific cooling (i.e. for non-isothermal melt-crystallization) or heating (i.e. for non-isothermal cold-crystallization) condition.

To use Equation (1) to analyze non-isothermal crystallization data obtained by DSC, it is assumed that the sample experiences a similar thermal history as designated by the DSC furnace. This may be realized when the lag between the temperatures of the sample and the furnace is minimal. If this assumption is valid, the relation between the crystallization time t and the sample temperature T can be written as

$$t = \frac{T_0 - T}{\phi},$$ (2)

where T_0 is an arbitrary reference temperature and ϕ is the cooling or heating rate. According to Equation (2), the horizontal temperature axis observed in a DSC thermogram for the non-isothermal crystallization data can be transformed into the time domain.

The most common approach to describe the overall isothermal crystallization kinetics is the Avrami model [19-21], in which the relative crystallinity as a function of time $\theta(t)$ can be expressed as

$$\theta(t) = 1 - \exp[-(K_A t)^{n_A}] \in [0,1],$$ (3)

where K_A and n_A are the Avrami crystallization rate constant and the Avrami exponent, respectively. Both K_A and n_A are constants specific to a given crystalline morphology and type of nucleation for a particular crystallization condition [22]. It should be noted that the units of K_A are given as an inverse of time. Although the Avrami equation is often used to describe the isothermal crystallization behavior of semi-crystalline polymers, it has also been applied to describe the non-isothermal crystallization behavior of semi-crystalline polymers [16-18,23,24].

A major drawback of the Avrami approach is that the model is only appropriate for describing only the early states of crystallization. Complications arise from the effects of growth site impingement and secondary crystallization process, which were disregarded for the sake of simplicity in the original derivation of the model. A theory for phase transformation kinetics with growth site

impingement was proposed by Tobin [25-27]. According to this approach, the relative crystallinity as a function of time $\theta(t)$ can be expressed as

$$\theta(t) = \frac{(K_T t)^{n_T}}{1 + (K_T t)^{n_T}} \in [0,1],$$

(4)

where K_T and n_T are the Tobin crystallization rate constant and the Tobin exponent, respectively. Based on this proposition, n_T needs not be an integer [25-27] and is also governed by different types of nucleation and growth mechanisms. It should be noted that the units of K_T are also given as an inverse of time.

Based on the mathematical derivation of Evans [28], Ozawa extended the Avrami theory to describe non-isothermal crystallization by assuming that the sample was cooled or heated with a constant rate from the molten or the glassy state) [29]. In the Ozawa method, the time variable in the Avrami equation was replaced by a cooling or heating rate and the relative crystallinity as a function of temperature $\theta(T)$ can be expressed as a function of cooling or heating rate ϕ as

$$\theta(T) = 1 - \exp[-\left(\frac{K_O}{\phi}\right)^{n_O}],$$

(5)

where K_O and n_O are the Ozawa crystallization rate constant and the Ozawa exponent, respectively. Both of the Ozawa kinetic parameters hold a similar physical meaning to those of the Avrami ones. Analytically, the Ozawa kinetic parameters can be extracted from a least-squared line drawn through the bulk of the data according to the double-logarithmic plot of $\ln[-\ln(1-\theta(T))]$ versus $\ln\phi$ for a fixed temperature, from which K_O and n_O can be determined from the y-intercept and the slope, respectively.

Instead of describing the crystallization process with complicated mathematical models, Ziabicki [30-32] proposed that the kinetics of polymeric phase transformation can be described by a first-order kinetic equation of the form:

$$\frac{d\theta(t)}{dt} = K_Z(T)[1 - \theta(t)],$$

(6)

where $K_Z(T)$ is a temperature-dependent crystallization rate function. In the case of non-isothermal crystallization, both $\theta(t)$ and $K_Z(T)$ functions vary and are dependent on the cooling rate used. For a given cooling or heating condition, Ziabicki [30-32]

showed that the crystallization rate function $K_Z(T)$ can be described by a Gaussian function of the following form:

$$K_Z(T) = K_{Z,max} \exp\left[-4\ln 2 \frac{(T - T_{max})^2}{D^2}\right],$$ (7)

where T_{max} is the temperature at which the crystallization rate is maximum, $K_{Z,max}$ is the crystallization rate at T_{max}, and D is the width at half-height of the crystallization rate function. With use of the iso-kinetic approximation, integration of Equation (7) over the whole crystallizable range (i.e. $T_g < T < T_m^0$) leads to an important characteristic value describing the crystallization ability of semi-crystalline polymers, i.e. the kinetic crystallizability index G_Z:

$$G_Z = \int_{T_g}^{T_m^0} K_Z(T)\,dT \approx 1.064 K_{Z,max} D.$$ (8)

According to the approximate theory [30], the parameter G_Z describes the ability of semi-crystalline polymers to crystallize when it is cooled at unit cooling or heating rate [32].

In case of non-isothermal crystallization studies using DSC, Equation (8) can be applied only when the crystallization rate function $K_Z(T)$ is replaced with a temperature-derivative of the relative crystallinity as a function of temperature [i.e. $(d\theta/dT)_\phi$] specific for each cooling or heating rate studied. As a result, Equation (8) now reads

$$G_{Z,\phi} = \int_{T_g}^{T_m^0} (d\theta/dT)_\phi\,dT \approx 1.064(d\theta/dT)_{\phi,max} D_\phi,$$ (9)

where $(d\theta/dT)_{\phi,max}$ and D_ϕ are the maximum crystallization rate and the width at half-height of the $(d\theta/dT)_\phi$ function. According to Equation (9), $G_{Z,\phi}$ is the kinetic crystallizability index for an arbitrary cooling or heating rate ϕ. The Ziabicki kinetic crystallizability index G_Z can finally be obtained by normalizing $G_{Z,\phi}$ with ϕ (i.e., $G_Z = G_{Z,\phi}/\phi$). This normalization was first proposed by Jeziorny [33].

For non-isothermal crystallization of semi-crystalline polymers, reliable values of the effective energy barrier can be obtained, for examples, by the differential iso-conversional method of Friedman [34] or by the integral iso-

conversional method of Vyazovkin [35-37]. In this work, the Friedman method was used, due largely to the reliability and simplicity of the method [36,37]. The Friedman equation is expressed as

$$\ln[\dot{\theta}_\theta(t)] = A - \frac{\Delta E_\theta}{RT}, \qquad (10)$$

where $\dot{\theta}_\theta(t)$ is the instantaneous crystallization rate as a function of time for a given value of relative crystallinity θ, A is an arbitrary pre-exponential parameter, and ΔE_θ is the effective energy barrier of the process for a given θ. By plotting the $\dot{\theta}_\theta(t)$ function obtained at under various cooling or heating rates against the corresponding inversed temperature for a given θ, the effective energy barrier for non-isothermal crystallization process can finally be determined.

3. EXPERIMENTAL DETAILS

3.1. Materials

The PTT sample used in this study was supplied in pellet form by Shell Chemicals Company (USA) (Corterra CP509201). The weight- and number-average molecular weights of this resin were kindly determined by Dr. Hoe Chuah and his colleagues of Shell Chemicals Company (USA), based on size-exclusion chromatography (SEC), to be ca. 78,100 and 34,700 Daltons, respectively.

3.2. Sample preparation and experimental procedure

PTT pallets were dried in a vacuum oven at 140°C for 5 hours prior to further use. Films of approximately 200 μm in thickness were obtained by melt-pressing dried pellets at 260°C in a Wabash V50H compression press under an applied hydraulic force of 10 tons. After 5 min holding time, the films were cooled down, while being in the compression press, to room temperature. The cooling of the platens of the compression press was by running cold water through channels in the platens and the cooling rate of the platens could be approximated by an exponential temperature-time decay, with a time constant of ca. 3 min.

A Perkin-Elmer Series 7 DSC (DSC-7) was used to study non-isothermal melt-crystallization kinetics of PTT. Temperature calibration was carried out using

an indium standard (T_m^0 = 156.6°C and ΔH_f^0 = 28.5 J g^{-1}). The consistency of the temperature calibration was checked every other run to ensure the reliability of the data obtained. To minimize thermal lag between the polymer sample and the DSC furnace, each sample holder was loaded with a disc-shaped specimen, weighing around 8.0 ± 0.5 mg, which was cut from the as-prepared films. Each sample was used only once and all the experimental runs were preformed under nitrogen atmosphere to minimize thermal degradation.

For non-isothermal crystallization from the glassy state, each sample was first heated from 25°C at a heating rate of 80°C·min^{-1} to 275°C and maintained at this temperature for 5 min to ensure complete melting [38]. After 5 minutes melt-annealing at 275°C, the sample was quickly taken out of the DSC cell and immediately quenched in liquid nitrogen, while still being in the DSC sample holder. After submersion in liquid nitrogen for 10 min, the sample was quickly transferred to the DSC cell where its temperature was set at 25°C to prevent the sample from premature crystallization (cf. the T_g of PTT at 44°C [39]). After temperature stabilization, the sample was heated from 25 to 275°C at a desired heating rate ϕ, ranging from 5 to 30°C·min^{-1} in order to observe the non-isothermal cold-crystallization and subsequent melting behavior of PTT.

4. RESULTS AND DISCUSSION

4.1. Non-isothermal cold-crystallization and subsequent melting behavior

The non-isothermal cold-crystallization exotherms of PTT recorded at eight different heating rates ranging from 5 to 30°C·min^{-1} are illustrated in Figure 1. Obviously, all of the major thermal transitions were observed in these exotherms. The glass transition was not found to be much affected by changes in the heating rate used, with the average value found in this work being 44.5 ± 0.5°C. which is in the vicinity of the reported value of 44°C [39]. The crystallization exotherm, however, became wider and shifted towards a higher temperature with increasing heating rate, as would be expected for crystallization in a diffusion-controlled region. In order to obtain some kinetic information quantitatively, it is necessary to convert these exotherms to the relative crystallinity as a function of temperature $\theta(T)$ using

Equation (1). The converted $\theta(T)$ curves are shown in Figure 2. Based on these curves, some kinetic data [e.g. the temperature at 1% relative crystallinity $T_{0.01}$, the temperature at the maximum crystallization rate (i.e. the peak temperature) T_p, and the temperature at 99% relative crystallinity $T_{0.99}$] can be obtained and these values are summarized in Table 1. Evidently, the $T_{0.01}$, T_p, and $T_{0.99}$ values all shifted towards higher temperatures when the heating rate increased. It should be noted that the $T_{0.01}$ and $T_{0.99}$ values are used here to represent the apparent onset and ending temperatures of the non-isothermal cold-crystallization process.

To further analyze the experimental data, the temperature scale of the obtained $\theta(T)$ curves need to be converted to the time scale, using Equation (2), to arrive at the relative crystallinity as a function of time $\theta(t)$. The converted $\theta(t)$ curves (the raw data are shown as various geometrical points) are presented in Figure 3. It is obvious, from Figure 3, that the total crystallization time decreased with increasing heating rate used. It is important to note that all of the $\theta(t)$ curves shown do not include the apparent incubation period Δt_{inc}, which is defined as a time period that a polymer sample spends from the temperature where it is brought to cold-crystallize (i.e. the initial temperature, T_{ini}) to the onset temperature where detectable crystallites are observed [viz. $\Delta t_{inc} = (T_{onset} - T_{ini})/\phi$, where, in this case, $T_{ini} = 25°C$]. The Δt_{inc} values for all of the heating rates studied are summarized in Table 2. Obviously, Δt_{inc} was found to monotonically decrease from ca. 6.9 min at 5°C·min^{-1} to ca. 1.5 min at 30°C·min^{-1}.

In order to quantify the bulk kinetics of the non-isothermal cold-crystallization process, the crystallization time at an arbitrary relative crystallinity (i.e. t_θ) can be determined from the $\theta(t)$ curves shown in Figure 3. The t_θ values after subtraction of the apparent incubation period Δt_{inc} for various values of the relative crystallinity θ (i.e. at the θ values of 0.01, 0.1, 0.3, 0.5, 0.7, 0.9, and 0.99, respectively) are summarized in Table 2 and are plotted as a function of heating rate in Figure 4. It should be noted that the $t_{0.01}$ and $t_{0.99}$ values are qualitative measures of the beginning and the ending of the non-isothermal cold-crystallization process. From these two values, the apparent total crystallization period Δt_c can be calculated (i.e. $\Delta t_c = t_{0.99} - t_{0.01}$) and the resulting values are summarized in Table 2.

Clearly, the way in which the t_θ value for a fixed value of θ and the Δt_c value were all found to decrease with increasing heating rate suggest that non-isothermal cold-crystallization proceeded faster with increasing the heating rate used. In an attempt to further analyze the results obtained, plots of $\ln(\Delta t_c)$ versus $\ln(\phi)$ (shown as the inset figure in Figure 4) and of $\ln(t_\theta)$ versus $\ln(\phi)$ for various values of θ (shown in Figure 5) were carried out. Apparently, a linear relationship is observed on these plots and, very interestingly, all of the plots exhibited a similar value of the slopes (see Table 3), with the average value being ca. -0.847 $min^2 \cdot {}^\circ C^{-1}$. These similar trends were also observed in the non-isothermal melt-crystallization of PTT, in which the average value of the slopes was found to be ca. -0.727 $min^2 \cdot {}^\circ C^{-1}$ [18].

The subsequent melting behavior after non-isothermal cold-crystallization of PTT can be observed directly from the results shown in Figure 1. Obviously, only double melting endotherms (for heating rates lower than or equal to $10^\circ C \cdot min^{-1}$) or single melting endotherm (for heating rates greater than or equal to $12.5^\circ C \cdot min^{-1}$) were visible. The low-temperature melting endotherm was found to decrease very slightly with increasing heating rate used (i.e. from ca. $225.7^\circ C$ at $5^\circ C \cdot min^{-1}$ to ca. $224.1^\circ C$ at $10^\circ C \cdot min^{-1}$, with the average value being $225.0 \pm 0.8^\circ C$). In a similar manner, the high-temperature melting was also found to decrease very slight with increasing heating rate used (i.e. from ca. $228.7^\circ C$ at $5^\circ C \cdot min^{-1}$ to ca. $226.6^\circ C$ at $30^\circ C \cdot min^{-1}$, with the average value being $227.5 \pm 0.8^\circ C$).

The subsequent melting behavior observed after non-isothermal cold-crystallization of PTT was totally different from that observed after non-isothermal melt-crystallization. In non-isothermal melt-crystallization of PTT [18], triple melting endotherms were visible in subsequent heating thermograms collected at cooling rates lower than or equal to $20^\circ C \cdot min^{-1}$, while double melting endotherms were observed at cooling rates greater than $20^\circ C \cdot min^{-1}$. Normally, the subsequent melting behavior of both isothermal melt-crystallization at temperatures lower than $194^\circ C$ [40] and non-isothermal melt-crystallization at cooling rates lower than or equal to $20^\circ C \cdot min^{-1}$ [18] showed triple melting endothermic behavior. These three endotherms were labeled as peaks I, II, and III for low-, middle-, and high-temperature melting endotherm [40]. Peak I was believed to correspond to the

melting of the primary crystallites formed and peaks II and III corresponded to the melting of the recrystallized crystallites of different stabilities which were simultaneously formed during the melting of the less stable primary crystals during a subsequent heating scan [40].

In comparison with these previous reports [18,40], the low- and the high-temperature melting endotherms observed after non-isothermal cold-crystallization corresponded to peaks II and III, with the similar average values being observed. The results suggest that the primary crystallites formed during non-isothermal cold-crystalllization were very unstable. During further heating, these unstable crystallites gradually melted over a wide temperature range, hence no peak I and no trace of small recrystallization exotherm were observed and only the melting endotherm(s) for the melting of recrystallized crystallites was (were) observed.

4.2. Non-isothermal cold-crystallization kinetics

4.2.1. Avrami analysis

Data analysis based on the Avrami macrokinetic equation was carried out by directly fitting the experimental $\theta(t)$ functions, shown as various geometrical points in Figure 3, to Equation (3), shown in Figure 3 as solid lines. The Avrami kinetic parameters (i.e. K_A and n_A) along with the r^2 parameter, signifying the goodness of the data fitting, were obtained from the best fits and the values of these parameters are summarized in Table 4. According to Table 4, n_A was found to range from ca. 5.0 to 5.9, with the average value being 5.4 ± 0.3. For non-isothermal melt-crystallization [18], n_A was found to range from ca. 4.4 to 4.7, with the average value being 4.6 ± 0.1. K_A was found to increase monotonically with increasing heating rate used, which is in general accordance with the values of the reciprocal half-time of crystallization $t_{0.5}^{-1}$ (i.e. the inverse value of t_θ when $\theta = 0.5$), which are also summarized in Table 4.

4.2.2. Tobin analysis

Data analysis based on the Tobin macrokinetic equation was carried out by directly fitting the experimental $\theta(t)$ functions, shown as various geometrical points

in Figure 3, to Equation (4), shown in Figure 3 as dotted lines. The Tobin kinetic parameters (i.e. K_T and n_T) along with the r^2 parameter, signifying the goodness of the data fitting, were obtained from the best fits and the values of these parameters are summarized in Table 4. According to Table 4, n_T was found to range from ca. 7.0 to 8.4, with the average value being 7.7 ± 0.5. For non-isothermal melt-crystallization [18], n_T was found to range from ca. 6.8 to 7.3, with the average value being 7.0 ± 0.2. K_T was, again, found to increase monotonically with increasing heating rate used, which is in general agreement with the K_A and $t_{0.5}^{-1}$ values obtained.

4.2.3. Comparison between results obtained from Avrami and Tobin analyses

A direct comparison between the results obtained form the two models suggests that both of the Avrami and the Tobin crystallization rate constants (i.e. K_A and K_T, respectively) are quite comparable, with the K_A value being the smaller of the two for a given heating rate. The results also show that, for a given heating rate, the value of n_A was always smaller than that of n_T, with the average value of the difference between the two parameters being 2.3 ± 0.2. In the case of non-isothermal melt-crystallization [18], the average value of the difference between the two parameters was found to be 2.5 ± 0.1.

The best way to observe the efficiency of both models in describing the non-isothermal cold-crystallization kinetics of PTT is to reconstruct the $\theta(t)$ functions from the results summarized in Table 4 according to Equations (3) and (4) for the Avrami and the Tobin models, respectively. The reconstructed $\theta(t)$ curves according to the Avrami and the Tobin models are shown in Figure 3 as solid and dotted lines, respectively. Qualitatively, it is obvious that the Tobin model provided a much better prediction of the experimental data than does the Avrami model (cf. the r^2 values listed in Table 4), which is in the opposite to the case of non-isothermal melt-crystallization where the Avrami model was found to provided a much better prediction [18]. The failure of the Avrami model in predicting the experimental data at high relative crystallinity values may be a result of the severe growth site

impingement which should be more severe in the case of non-isothermal cold-crystallization in comparison to the case of non-isothermal melt-crystallization.

4.2.4. Ozawa analysis

By simply replacing t in Equation (1) with T/ϕ, Ozawa [29] was able to extend the Avrami model to describe the kinetics of non-isothermal crystallization. In this approach, the raw data is the relative crystallinity function of temperature $\theta(T)$ such as those shown in Figure 2. Data analysis according to this model can be carried out through a plot of $\ln[-\ln(1-\theta(T))]$ versus $\ln(\phi)$ for a fixed temperature, where n_O is taken as the negative value of the slope and K_O is taken as the antilogarithmic value of the ratio of the y-intercept and n_O [i.e. $K_O = \exp(y-\mathrm{intercept}/n_O)$]. Figure 6 shows typical Ozawa plots from the raw data shown in Figure 2 within the temperature range of 65 to 76°C, while Table 5 summarizes the Ozawa kinetic parameters (i.e. K_O and n_O), including the r^2 parameter. Qualitatively, the Ozawa model was satisfactory in describing the non-isothermal cold-crystallization data of PTT. According to Table 5, n_O was found to vary between 3.6 and 4.9, with the average value being 4.3 ± 0.4, while K_O was found to increase with increasing temperature, as would be expected for crystallization in the diffusion-controlled region.

4.2.5. Ziabicki's crystallizability analysis

Analysis according to the modified first-order Ziabicki's kinetic equation (i.e. Equation 9) can be carried out by differentiating the relative crystallinity as a function of temperature $\theta(T)$, such as those shown in Figure 2, with respect to temperature in order to obtain the derivative relative crystallinity as a function of temperature $(d\theta/dT)_\phi$. Once the $(d\theta/dT)_\phi$ function is obtained, various kinetic parameters (i.e. the maximum crystallization rate $(d\theta/dT)_{\phi,\mathrm{max}}$ and the width at half-height of the $(d\theta/dT)_\phi$ function D_ϕ) can then be obtained and the cooling rate-dependent kinetic crystallizability $G_{Z,\phi}$ can be calculated according to Equation (9). Table 6 summarizes values of $T_{\mathrm{max},\phi}$ (i.e. the temperature at the maximum crystallization rate as determined from the $(d\theta/dT)_\phi$ function), $(d\theta/dT)_{\phi,\mathrm{max}}$, D_ϕ, $G_{Z,\phi}$,

and, finally, G_Z. It should be noted that the values of $T_{max,\phi}$ listed in Table 6 and T_p (i.e. the temperature at the maximum crystallization rate as determined from the raw non-isothermal melt-crystallization exotherms) listed in Table 1 are identical. According to Table 6, the $T_{max,\phi}$, $(d\theta/dT)_{\phi,max}$, D_ϕ, and $G_{Z,\phi}$ values were all found to increase with increasing heating rate. After normalizing $G_{Z,\phi}$ value with the heating rate, the value of the kinetic crystallizability at unit cooling rate G_Z can be determined and the results summarized in Table 6 confirm that the normalized G_Z values obtained for different heating rates were almost identical, with the average value being 0.89 ± 0.01.

4.2.6. Effective energy barrier based on the differential iso-conversional method of Friedman

Analysis based on the differential iso-conversional method of Friedman starts with the conversion of a $\theta(T)$ function, such as those shown in Figure 2, into a $\theta(t)$ function, such as those shown in Figure 3. The converted $\theta(t)$ function is then differentiated with respect to time to obtain the instantaneous crystallization rate function of time $\dot{\theta}(t)$. A plot according to Equation (10) can then be performed for various values of relative crystallinity θ using the data obtained from the $\dot{\theta}(t)$ and the $\theta(T)$ functions and, finally, the effective energy barrier for non-isothermal cold-crystallization process for a given value of θ (i.e. ΔE_θ) can be determined, as a result, from the slope of the plot [i.e. $\Delta E_\theta = -(\text{slope})(R)$]. The ΔE_θ values determined for various values of θ, ranging from 0.1 to 0.9 with 0.1 increment, are summarized in Table 7. Apparently, ΔE_θ was found to range between ca. 114.5 and 158.8 kJ·mol⁻¹.

5. CONCLUSIONS

The non-isothermal cold-crystallization kinetic and the subsequent melting behavior of PTT for eight different cooling rates were investigated. The non-isothermal melt-crystallization exotherms of PTT showed that the temperature at 1% relative crystallinity, the temperature at the maximum crystallization rate, and the

temperature at 99% relative crystallinity were all shifted towards higher temperatures with an increase in the heating rate investigated, indicating that PTT took a longer time to crystallize as heating rate increased. Further analysis of the non-isothermal cold-crystallization behavior revealed that the apparent incubation period, the crystallization time at different relative crystallinity values, and the apparent total crystallization period were all found to decrease with increasing heating rate. Interestingly, both the crystallization time at different relative crystallinity values and the apparent total crystallization period showed a linear relationship with the heating rate in the log-log plots, with all the plots exhibiting a regression line of similar slope (i.e. the average value being ca. -0.847 $min^2 \cdot {}^\circ C^{-1}$). The subsequent melting behavior after non-isothermal cold-crystallization of PTT was found to exhibit either double melting behavior (for heating rates lower than or equal to $10^\circ C \cdot min^{-1}$) or single melting behavior (for heating rates greater than or equal to $12.5^\circ C \cdot min^{-1}$).

The Avrami and the Tobin models were all found to describe the non-isothermal cold-crystallization data of PTT fairly well, with the Tobin model being the better of the two. The average values of the Avrami and the Tobin exponents are ca. 5.4 and 7.7, respectively. Both the Avrami and Tobin crystallization rate constants were found to increase with increasing heating rate. The Ozawa model was also found to describe the non-isothermal cold-crystallization data of PTT fairly well. The Ozawa crystallization rate constant was found to be an increasing function of temperature, within the temperature range investigated. The ability for PTT to crystallize from the glassy state under a unit heating rate was evaluated based on the Ziabicki's kinetic crystallizability, from which it was found to be ca. 0.89. Lastly, the effective energy barrier governing the non-isothermal cold-crystallization of PTT was found to range between ca. 114.5 and 158.8 $kJ \cdot mol^{-1}$.

ACKNOWLEDGEMENTS

REFERENCES

[1] Whinfield JR and Dickson JT, *Brit Pat* 578,079 (14 June 1946).

[2] Process Economics Program Report: 227. 1,3-Propanediol and Poly(trimethylene terephthalate), SRI International (1999).

[3] Ward IM and Wilding MA, *J Polym Sci – Polym Phys* 14:263 (1976).

[4] Chuah H, in Scheirs J and Long T (Eds), Modern Polyesters, John Wiley & Sons, New York, 2003 (Chapter 11).

[5] Supaphol P and Spruiell JE, *Polymer* 42:699 (2001).

[6] Qiu ZB, Ikehara T, and Nishi T, *Polymer* 44:3429 (2003).

[7] Jakeways R, Ward IM, and Wilding MA, *J Polym Sci – Polym Phys* 13:799 (1975).

[8] Ho RM, Ke KZ, and Chen M, *Macromolecules* 33:7529 (2000).

[9] Wang B, Li CY, Hanzlicek J, Cheng SZD, Geil PH, Grebowicz J, and Ho RM, *Polymer* 42:7171 (2001).

[10] Chuah HH, *Polym Engng Sci* 41:308 (2001).

[11] Huang JM and Chang FC, *J Polym Sci – Polym Phys* 38:934 (2000).

[12] Hong PD, Chung WT, and Hsu CF, *Polymer* 43:3335 (2002).

[13] Wang XS, Yan D, Tian GH, and Li XG, *Polym Engng Sci* 41:1655 (2001).

[14] Dangseeyun N, Srimoaon P, Supaphol P, and Nithitanakul M, *Thermochim Acta 409*:77 (2004).

[15] Chen M, Chen CC, Ke KZ, and Ho RM, *J Macromol Sci – Phys* 41:1063 (2002).

[16] Supaphol P, Dangseeyun N, Srimoaon P, and Nithitanakul M, *Thermochim Acta* 406:207 (2003).

[17] Supaphol P, Dangseeyun N, and Srimoaon P, *Polym Test* 23:175 (2004).

[18] Apiwanthanakorn N, Supaphol P, and Nithitanakul M, *Polym Test*, accepted.

[19] Avrami M, *J Chem Phys* 7:1103 (1939).

[20] Avrami M, *J Chem Phys* 8:212 (1940).

[21] Avrami M, *J Chem Phys* 9:177 (1940).

[22] Wunderlich B, in Macromolecular Physics, Vol. 2, Academic Press, New York, 1976, p. 147.

[23] Supaphol P, *J Appl Polym Sci* **78**:338 (2000).

[24] Zhang QX, Zhang ZH, Zhang HF, and Mo ZS, *J Polym Sci – Polym Phys* **40**:1784 (2002).

[25] Tobin MC, *J Polym Sci – Polym Phys* **12**:399 (1974).

[26] Tobin MC, *J Polym Sci – Polym Phys* **14**:?253 (1976).

[27] Tobin MC, *J Polym Sci – Polym Phys* **15**:2269 (1977).

[28] Evans UR, *Trans Faraday Soc* **41**:365 (1945).

[29] Ozawa T, *Polymer* **12**:150 (1971).

[30] Ziabicki A, *Appl Polym Symp* **6**:1 (1967).

[31] Ziabicki A, *Polymery* **12**:405 (1967)

[32] Ziabicki A, in Fundamentals of Fiber Spinning, John Wiley & Sons, New York, 1976, pp 112-114.

[33] Jeziorny A, *Polymer* **19**:1142 (1978).

[34] Friedman H, *J Polym Sci* **C6**:183 (1964-1965).

[35] Vyazovkin S, *J Comput Chem* **18**:393 (1997).

[36] Vyazovkin S, *J Comput Chem* **22**:178 (2001).

[37] Vyazovkin S, *Macromol Rapid Commun* **23**:771 (2002).

[38] Supaphol P, Srimoaon P, and Sirivat A, *Polym Int*, accepted.

[39] Supaphol P, Dangseeyun N, Thanomkiat P, and Nithitanakul M, *J Polym Sci – Polym Phys* **42**:676 (2004).

[40] Srimoaon P, Dangseeyun N, and Supaphol P, *Eur Polym J* **40**:599 (2004).

CAPTION OF FIGURES

Figure 1.   Non-isothermal cold-crystallization exotherm and subsequent melting behavior of PTT at eight different cooling rates.

Figure 2.   Relative crystallinity as a function of temperature of PTT at eight different cooling rates. These curves have been converted from the data shown in Figure 1 using Equation (1).

Figure 3.   Relative crystallinity as a function of time of PTT for eight different cooling rates. These curves have been converted from the data shown in Figure 2 using Equation (2). Different geometrical points represent the raw data, while the solid and the dotted lines are the Avrami and the Tobin predictions, respectively.

Figure 4.   Crystallization time at various relative crystallinity values as a function of cooling rate. The inset figure shows relationship between apparent total crystallization period and cooling rate in a log-log plot.

Figure 5.   Relationship between crystallization time at various relative crystallinity values and cooling rate in a log-log plot.

Figure 6.   Typical Ozawa analysis based on the non-isothermal cold-crystallization data of PTT.

Table 1. Characteristic data of non-isothermal cold-cystallization exotherms for PTT.

ϕ (°C min^{-1})	$T_{0.01}$ (°C)	T_p (°C)	$T_{0.99}$ (°C)
5.0	61.8	65.8	71.4
7.5	63.6	67.6	72.7
10.0	64.3	68.6	74.4
12.5	65.3	70.0	75.8
15.0	67.0	71.3	77.8
20.0	68.9	73.3	79.9
25.0	69.5	74.1	81.7
30.0	71.6	76.0	84.2

Table 2. Quantitative analysis of the relative crystallinity functions of time which were converted from non-isothermal cold-crystallization data of PTT.

ϕ (°C·min^{-1})	Δt_{inc} (min)	t_θ (min)							Δt_c (min)
		$\theta = 0.01$	$\theta = 0.1$	$\theta = 0.3$	$\theta = 0.5$	(min)	$\theta = 0.9$	$\theta = 0.99$	
5.0	6.85	0.51	0.91	1.15	1.29	1.42	1.70	2.44	1.93
7.5	4.79	0.35	0.63	0.79	0.88	0.97	1.14	1.57	1.21
10.0	3.65	0.29	0.50	0.63	0.70	0.78	0.92	1.30	1.01
12.5	2.96	0.27	0.45	0.56	0.63	0.69	0.80	1.10	0.84
15.0	2.55	0.25	0.40	0.49	0.54	0.59	0.69	0.97	0.72
20.0	2.02	0.17	0.29	0.36	0.40	0.44	0.52	0.72	0.55
25.0	1.65	0.13	0.23	0.28	0.32	0.36	0.43	0.62	0.49
30.0	1.45	0.11	0.19	0.24	0.27	0.30	0.37	0.53	0.42

Table 3. Y-intercept, slope, and the r^2 values of regression lines drawn through plots of $\ln(t_0)$ against $\ln(\phi)$ for various relative crystallinity values.

θ	Y-intercept (min)	slope (min^2 °C^{-1})	r^2
0.01	0.71	-0.839	0.972
0.1	1.30	-0.854	0.989
0.3	1.53	-0.857	0.993
0.5	1.64	-0.855	0.995
0.7	1.72	-0.850	0.996
0.9	1.87	-0.844	0.997
0.99	2.19	-0.830	0.996
	Average	-0.847	

Table 4. Non-isothermal cold-crystallization kinetics for PTT based on Avrami and Tobin analyses.

ϕ ($^\circ$C min^{-1})	$t_{0.5}^{-1}$ (min^{-1})	Avrami analysis			Tobin analysis		
		n_A	K_A (min^{-1})	r^2	n_T	K_T (min^{-1})	r^2
5.0	0.78	5.21	0.720	0.9987	7.30	0.785	0.9995
7.5	1.13	5.33	1.054	0.9992	7.84	1.145	0.9994
10.0	1.42	5.30	1.317	0.9990	7.54	1.432	0.9996
12.5	1.60	5.64	1.487	0.9991	8.16	1.609	0.9995
15.0	1.86	5.93	1.735	0.9989	8.35	1.872	0.9996
20.0	2.50	5.47	2.325	0.9991	7.91	2.527	0.9996
25.0	3.13	5.06	2.871	0.9987	7.21	3.143	0.9997
30.0	3.69	4.97	3.385	0.9987	6.93	3.714	0.9997

Table 5. Non-isothermal cold-crystallization kinetics for PTT based on Ozawa analysis.

Temperature (°C)	PTT		
	n_O	K_O (°C min^{-1})	r^2
65	4.08	3.82	0.9861
66	4.00	4.84	0.9926
67	3.63	5.89	0.9907
68	3.77	7.03	0.9199
69	4.38	9.25	0.9255
70	4.63	10.51	0.9545
71	4.74	12.78	0.9752
72	4.74	14.22	0.9434
73	4.62	16.75	0.9409
74	4.37	19.57	0.9007
75	4.90	23.36	0.8665
76	3.84	26.37	0.8562

Table 6. Non-isothermal cold-crystallization kinetics for PTT based on Ziabicki's kinetic crystallizability analysis.

ϕ (°C min^{-1})	$T_{max,\phi}$ (°C)	$(d\theta/dT)_{\phi,ma}$ $_x$ (min^{-1})	D_ϕ (°C)	$G_{Z,\phi}$ (°C min^{-1})	G_Z
5.0	65.8	1.54	2.68	4.37	0.87
7.5	67.6	2.26	2.77	6.67	0.89
10.0	68.6	2.74	3.04	8.88	0.89
12.5	70.0	3.28	3.19	11.14	0.89
15.0	71.3	3.93	3.20	13.35	0.89
20.0	73.3	4.78	3.55	18.07	0.90
25.0	74.1	5.40	3.93	22.61	0.90
30.0	76.0	5.92	4.32	27.23	0.91
				Average	0.89

Table 7. Effective energy barrier describing the overall non-isothermal cold-crystallization of PTT based on the differential iso-conversional method of Friedman.

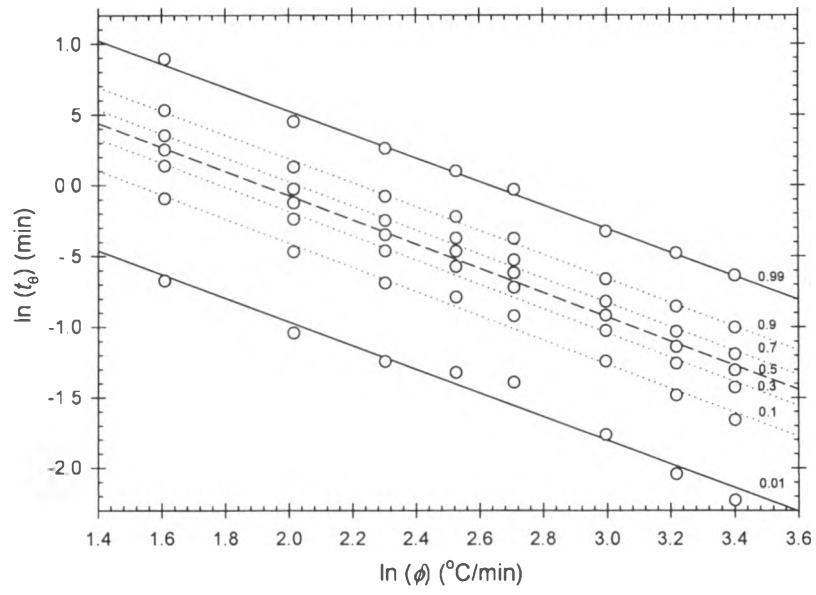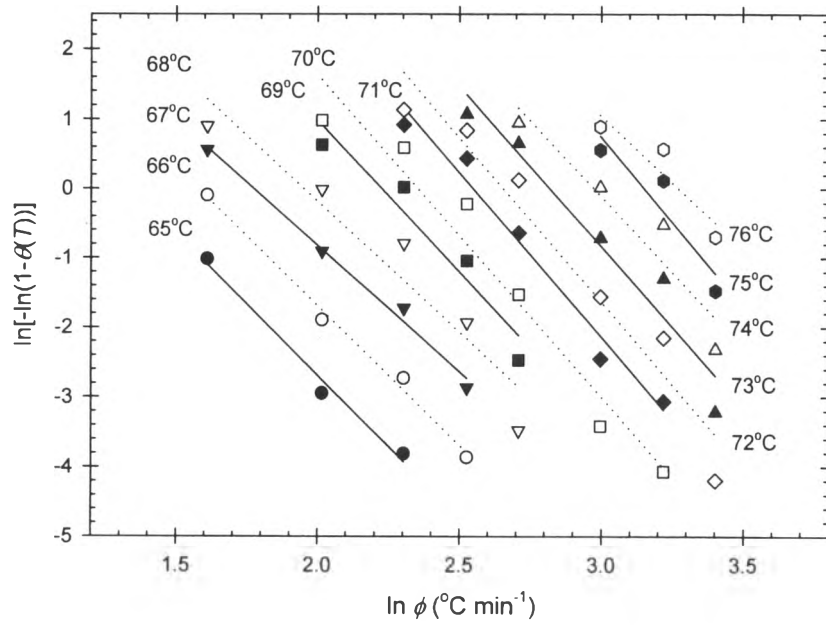| θ	ΔE_θ (kJ mol^{-1})	r^2
0.1	158.8	0.983
0.2	147.9	0.980
0.3	137.5	0.972
0.4	128.4	0.965
0.5	120.9	0.958
0.6	115.8	0.951
0.7	114.5	0.945
0.8	119.6	0.938
0.9	141.1	0.932
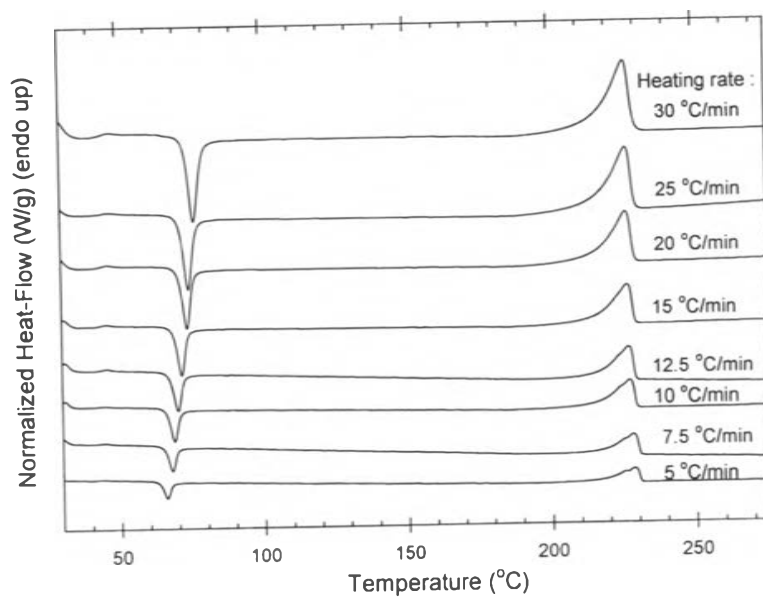
Figure 1
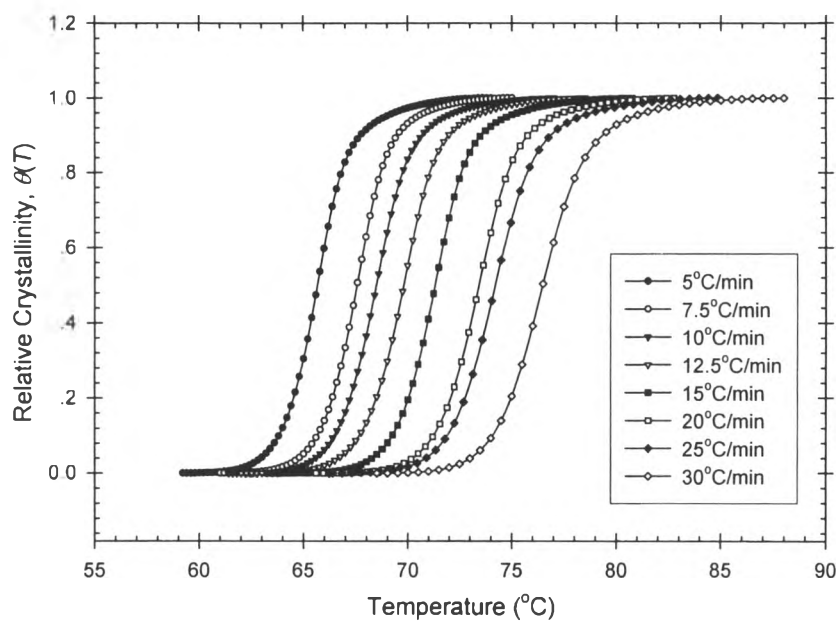
Figure 2
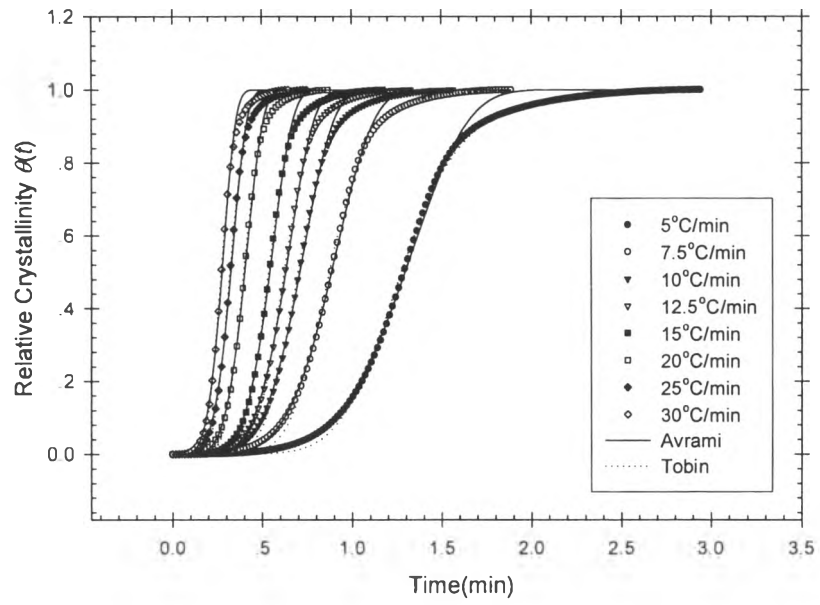
Figure 3
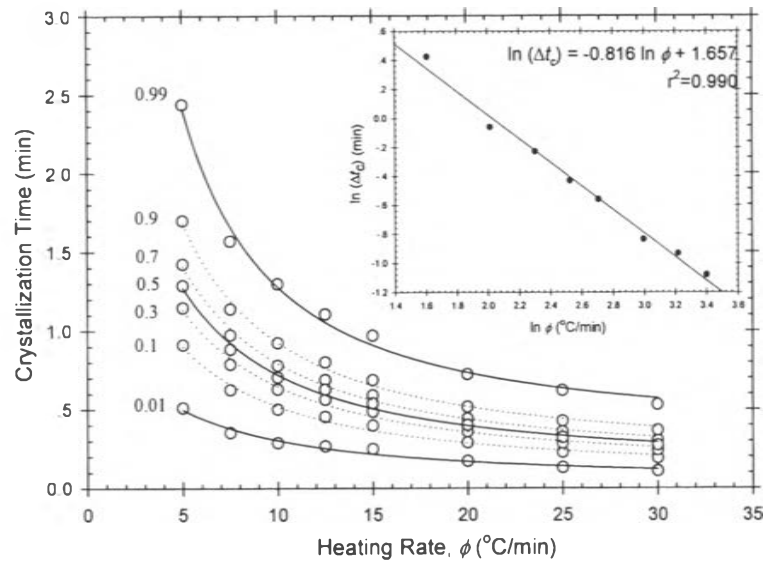
Figure 4

Figure 5

Figure 6